

RESEARCH ARTICLE | SEPTEMBER 07 2016

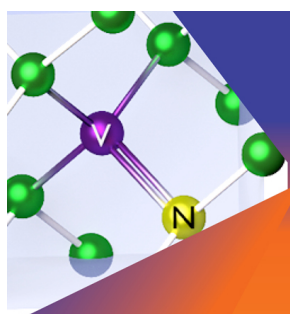
Modification of the phonon spectrum of bulk Si through surface nanostructuring

A. Iskandar; A. Gwiazda; Y. Huang; M. Kazan; A. Bruyant; M. Tabbal; G. Lerondel



J. Appl. Phys. 120, 095106 (2016)

<https://doi.org/10.1063/1.4962208>



Applied Physics Letters | Journal of Applied Physics

Special Topic:

Defects in Solids for Quantum Technologies

Guest Editors: Adam Gali, Viktor Ivády, Igor Abrikosov and Yuan Ping

Submit Today!

Modification of the phonon spectrum of bulk Si through surface nanostructuring

A. Iskandar,^{1,2} A. Gwiazda,² Y. Huang,² M. Kazan,^{1,a)} A. Bruyant,² M. Tabbal,¹ and G. Lerondel²

¹Department of Physics, American University of Beirut, P.O. Box 11-0236, Riad El-Solh, Beirut 1107-2020, Lebanon

²Laboratoire de Nanotechnologie et d'Instrumentation Optique, ICD, CNRS UMR 6281, Université de Technologie de Troyes, 10010 Troyes, France

(Received 25 July 2016; accepted 22 August 2016; published online 7 September 2016)

In this paper, we present experimental evidence on the change of the phonon spectrum and vibrational properties of a bulk material through phonon hybridization mechanisms. The phonon spectrum in a finite material is strongly affected by the presence of free surfaces, which is the addition of a contribution from an essentially two-dimensional crystal. The phonon spectrum of a bulk material can hence be altered by a hybridization mechanism between confined phonon modes in nanostructures introduced on the surface of a bulk material and the underlying bulk phonon modes. We measured the heat capacities of bare and surface-structured silicon substrates originating from the same silicon wafer. Then, we deduced important features of the phonon spectra of the samples investigated through a rigorous analysis of the measured heat capacity curves. The results show that the shape and size of the nanostructures made on the surface of the bulk substrate have a strong effect on the phonon spectrum of the bulk material. *Published by AIP Publishing.*

[<http://dx.doi.org/10.1063/1.4962208>]

I. INTRODUCTION

Efficient thermal management is often considered as a key step towards a successful technological system. The fast removal of excess heat from electronic systems exposed to temperature extremes improves the reliability and prevents premature aging and failure of these systems. On the contrary, maintaining a high temperature difference between the two sides of a thermoelectric module can significantly enhance the thermal energy harvesting through the direct recovery of waste heat and its conversion into useful electrical energy. Nowadays, the usual approaches to evacuate heat and maintain the system at a desired temperature consist in using a heat sink or a complex fan speed control system that relies on continuous temperature measurement.^{1,2} However, with the continuous reduction in the size of the devices and their time scales, the applicability of these basic approaches to ensure adequate system cooling becomes questionable. In thermoelectricity, the current trend is nanosizing and nanoengineering semiconductor materials in order to scatter the phonons (heat carriers) without intensely affecting the motion of electrons.^{3–7} Although this approach has demonstrated potential in creating nanoengineered materials that are somewhat efficient in thermal insulation while conserving their high electrical conduction, it did not lead to the development of solid-state based alternative energy technologies, mostly because the phonon scattering centers in these materials also scatter electrons and increase the ohmic heating.

As schematically depicted in Fig. 1, one way to circumvent this problem would be to find means to directly modify

the phonon spectrum of the material via phonon hybridization mechanisms between bulk phonon modes and confined phonon modes introduced on the material surface. With such a technology in hand, one could enhance the material thermal conductivity for fast heat removal or rationally reduce the thermal conductivity of a thermoelectric material without the inclusion of phonon scattering centers and boundaries that may undesirably cause obstruction to the electron transport and reduce the thermoelectric conversion efficiency. It was first shown by Weyl that the asymptotic distribution of normal mode frequencies is independent from the body shape provided that the size of the body is sufficiently large.⁸ According to Weyl, the error terms will always be of an order involving the ratio of the number of atoms in the surface to the total number in the solid and hence go to zero as the size of the solid increases without limit. The distribution of the eigenvalues of the differential equation describing the material vibrations is thus independent from the shape of the boundary of the region to which the eigenvalues correspond. Consequently, thermodynamic properties and phonon spectrum of solids are independent of the sample boundary shape. Therefore, at a first glance, it seems impossible to considerably alter the phonon spectrum of a bulk material by surface processing. However, stimulated by the theoretical work of Davis and Hussein,⁹ we demonstrate here experimentally that the phonon spectrum of a crystalline substrate can be altered by a hybridization mechanism between the confined phonon modes in nanostructures made on the surface and the underlying bulk lattice dispersion. The phonon hybridization mechanism has been recently intensively studied in nano-sized materials.^{10–15} Atomistic simulations of hybridization mechanisms in bulk materials would be extremely challenging.

^{a)}Author to whom correspondence should be addressed. Electronic mail: mk140@aub.edu.lb

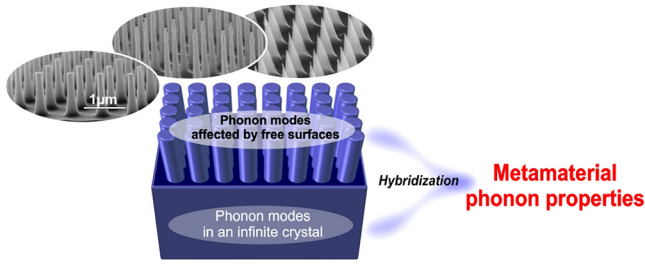


FIG. 1. Phonon hybridization mechanism and sketch of typical investigated Si nanostructured samples.

Therefore, we investigate the hybridization mechanism in bulk materials experimentally. By measuring the heat capacity of surface-structured Si substrates, we demonstrate in this paper that confined phonon modes may also hybridize with the phonon dispersion of an underlying bulk material, causing important modifications in the phonon spectrum and thermodynamic properties.

II. EXPERIMENTS

Phosphorus-doped ($2.28 \times 10^{17} \text{cm}^{-3} < N_d < 4.48 \times 10^{18} \text{cm}^{-3}$) silicon nanocones were fabricated by reactive-ion etching (RIE) using a hard mask. Laser interference lithography (laser wavelength used: 355 nm) was employed to define the mask patterns. A square lattice with circular patterns of period 700 nm was created by a double exposure of the samples, whereby the diameter of the features was varied from 280 nm to 460 nm by changing the exposure time. Thereafter, silicon etching was conducted in a Plassys MU400 reactor using a SF_6/O_2 gas mixture. Structures with a height varying between 400 nm and 1 μm were obtained by increasing the etching time. The nanostructures investigated in this work are sketched in Fig. 1.

Many different techniques for measuring the heat capacity are optimized for different sample sizes and accuracy requirements.¹⁶ The measurements of the heat capacity of the samples investigated in this work were performed by using the Quantum Design Physical Properties Measurement System that uses a relaxation technique combining accurate heat capacity measurement with a reliable analysis technique. After each measurement cycle, which is a heating period followed by a cooling period, the system fits the entire temperature response of the sample platform to a model that accounts for both the thermal relaxation of the sample platform to the bath temperature and the relaxation between the sample platform and the sample itself.¹⁷ In the case when the thermal connection shared by the sample and platform is poor, the system models the effect of the relaxation between the platform and the sample and reports the correct heat capacity values despite poor contact.

The system first assumes that the sample and sample platform are in good thermal contact with each other and are at the same temperature during the measurement period. In that simple case, the temperature T of the platform as a function of time t obeys the equation

$$C_{total} \frac{dT}{dt} = -\kappa_w(T - T_b) + P(t), \quad (1)$$

where C_{total} is the total heat capacity of the sample and sample platform, κ_w is the thermal conductivity of the supporting wires, T_b is the temperature of the thermal bath, and $P(t)$ is the power applied by the heater. The heater power $P(t)$ is equal to P_0 during the heating portion of the measurement and equal to zero during the cooling portion. The solution of this equation is given by exponential functions with a characteristic time constant τ equal to $\frac{C_{total}}{\kappa_{total}}$, where κ_{total} is the thermal conductivity of the sample and the sample platform.

The system generally uses Eq. (1) to measure most samples as well as the addenda (the sample holder and grease). However, when the thermal contact between the sample and the sample platform is poor, the system automatically simulates the effect of heat flowing between the sample platform and the sample by using a two-time-constant model and fits the entire temperature response accordingly. In the two-time-constant model, the temperature of the platform T_p and the temperature of the sample T_s obey the equations

$$C_{platform} \frac{dT_p}{dt} = P(t) - \kappa_w(T_p(t) - T_b) + \kappa_g(T_s(t) - T_p(t)), \quad (2)$$

and

$$C_{sample} \frac{dT_s}{dt} = -\kappa_g(T_s(t) - T_p(t)). \quad (3)$$

Here, $C_{platform}$ is the heat capacity of the sample platform, C_{sample} is the heat capacity of the sample, and κ_g is the thermal conductivity of the grease between the sample platform and the sample.

We set the measurement time way longer than the amount of time it takes for the sample to reach internal thermal equilibrium to avoid the effect of the thermal path and achieve accurate heat capacity measurement. The reproducibility of the measurements was checked by measuring each sample several times. All the recorded data for the same sample were identical within 1% of the heat capacity value.

III. RESULTS AND DISCUSSION

We measured the constant pressure heat capacity of the bare silicon (Si) substrate and eight Si structured substrates with truncated cone-like Si structures over 3–300 K temperature range. All the measured samples were obtained from the same Si wafer, and the surface structuration was made at low temperatures and with appropriate care to prevent any impurity diffusion or defect formation in the Si structures. The measured curves are presented in Fig. 2. The measurement uncertainty is indicated by the size of the symbols used to plot the data. As can be noticed, the measured data for the surface-structured samples differ from those of the bare Si substrate. This difference in heat capacity is due to differences in the samples harmonic vibration properties or differences in the properties of the electron gas in the samples. In the following discussion of the measurements, we refer to the constant volume specific heat, which is a direct measurement of the constant volume heat capacity times the mass of the measured sample, for convenience. Since constant

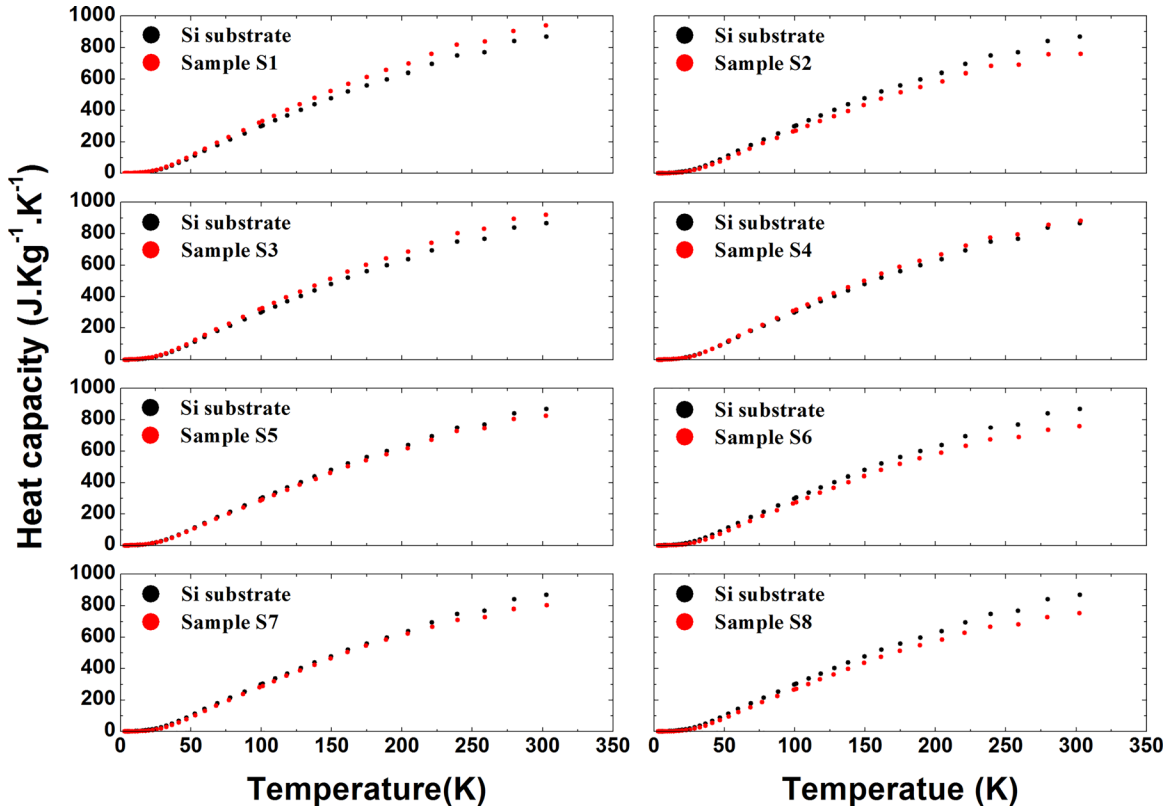


FIG. 2. Heat capacity measurements of the samples investigated.

volume is hard to arrange experimentally, we measure the heat capacity at constant pressure. However, one can readily show that at room temperature and below, the ratio of the solid constant pressure specific heat to its constant volume specific heat is very close to one.

At a few degrees Kelvin, where the crystal chemical potential coincides with the Fermi energy, the crystal constant volume specific heat is given by

$$C_v = \left(\frac{\partial E_t}{\partial T} \right)_v = \frac{\pi^2 k_B^2 n}{2\varepsilon_F} T + 3rNk_B \frac{4\pi^2}{5} \left(\frac{T}{\theta_D} \right)^3, \quad (4)$$

where E_t is the total energy of the sample, k_B is the Boltzmann constant, n is the concentration of free carriers, ε_F is the Fermi energy, r is the number of atoms per unit cell, N is the number of unit cells in the sample, and θ_D is the Debye temperature. The first and second terms on the right hand side in Eq. (4) represent the contribution of the electron gas and the contribution of the lattice harmonic dynamics to the total specific heat, respectively. The lattice dynamics contribution completely dominates the specific heat at high temperatures. However, well below room temperature, the lattice dynamics contribution falls off as the cube of the temperature, and at very low temperatures, it drops and may become comparable to the electronic contribution, which only decreases linearly with temperature. In order to separate out these two contributions, we write Eq. (4) as $\frac{C_v}{T} = \gamma + AT^2$ and plot $\frac{C_v}{T}$ versus T^2 . Then, we find γ by extrapolating the $\frac{C_v}{T}$ curve linearly down to $T^2 = 0$, and noting where it intercepts the $\frac{C_v}{T}$ -axis. The linear extrapolations of all the $\frac{C_v}{T}$ curves are shown together in Fig. 3, and the deduced γ values are presented in Table I. The obtained small

values of γ clearly demonstrate the absence of observable contribution of the electron gas to the specific heat in all the measured samples. Therefore, we can confidently consider that the lattice harmonic dynamics of the samples are the only determinants of their specific heats. This allows writing the total constant volume specific heat as an additive function of the normal modes frequencies $\omega_j(k)$ in the form

$$C_v = \left(\frac{\partial E}{\partial T} \right)_v = k_B \sum_{kj} \frac{\left(\frac{\hbar\omega_j(k)}{2k_B T} \right)^2}{\sinh^2 \left(\frac{\hbar\omega_j(k)}{2k_B T} \right)}, \quad (5)$$

where the summation runs over all the phonon states (\sum_k) and polarizations (\sum_j). This has the consequence that the

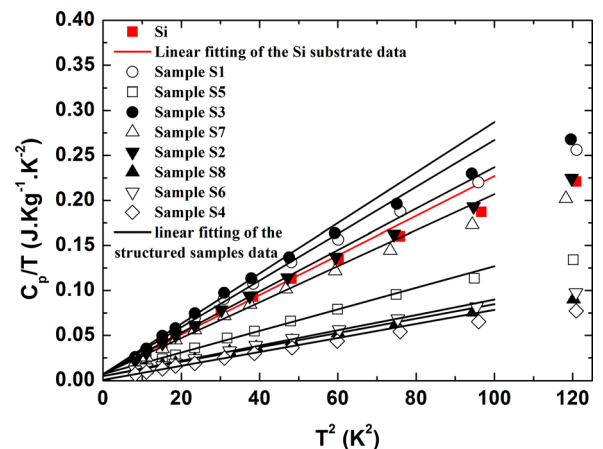








FIG. 3. $\frac{C_p}{T}$ versus T^2 . Symbols: Measurements. Solid lines: Extrapolation of $\frac{C_p}{T}$ down to $T^2 = 0$.

TABLE I. The characteristics of the samples investigated and the parameters of their phonon spectra obtained from the analysis of the specific heat measurements.

Sample	Structure	Structure bottom diameter (nm)	Structure top diameter (nm)	Structure height (nm)	Structure volume (nm ³)	γ	θ_0 (K)	$a_2 \times 10^{-42}$	$a_4 \times 10^{-70}$	Spectrum moments
Bare Si substrate	0.007	625	5.05	-4501	$u_2 = 0.850$ $u_4 = 0.720$ $u_6 = 0.300$
	S1	134	15	450	2 378 696	0.0070	600	6.1894	-3901	$u_2 = 0.695$ $u_4 = 0.450$ $u_6 = 0.145$
	S2	453	413	592	87 236 076	0.0070	750	3.1690	-230	$u_2 = 0.840$ $u_4 = 0.780$ $u_6 = 0.355$
	S3	334	43	800	26 759 458	0.0070	590	6.5094	-475	$u_2 = 0.760$ $u_4 = 0.540$ $u_6 = 0.190$
	S4	380	235	875	66 185 340	0.0005	650	4.8681	-345	$u_2 = 0.690$ $u_4 = 0.460$ $u_6 = 0.150$
	S5	265	60	1000	23 489 950	0.0070	625	5.4760	-4101	$u_2 = 0.930$ $u_4 = 0.870$ $u_6 = 0.400$
	S6	450	100	1150	77 525 343	0.0048	870	2.0302	-128	$u_2 = 0.670$ $u_4 = 0.530$ $u_6 = 0.205$
	S7	291	159	1240	50 717 463	0.0070	855	2.1390	-120	$u_2 = 0.580$ $u_4 = 0.380$ $u_6 = 0.123$
	S8	650	190	1280	195 063 582	0.0048	933	1.6461	-85	$u_2 = 0.610$ $u_4 = 0.445$ $u_6 = 0.160$

specific heat can be expressed as average over the phonon spectrum $g(\omega)$ as

$$C_v = 3rNk_B \int_0^{\omega_L} \left(\frac{\hbar\omega}{2k_B T} \right)^2 \operatorname{csch}^2 \left(\frac{\hbar\omega}{2k_B T} \right) g(\omega) d\omega, \quad (6)$$

where ω_L is the frequency that determines the upper limit of the phonon band. In the following, we make use of the heat capacity measurements and Eq. (6) to estimate the effect of the confined phonon modes on some important features of $g(\omega)$.

A. Effect of phonon hybridization mechanisms on the low frequency end of the phonon spectrum

Let us investigate first the effect of surface nanostructuring on the low frequency end of the phonon spectrum. At low temperatures, the expression for the specific heat, Eq. (6), takes the form

$$C_v(T) = 3rNk_B \int_0^{\omega_L} \left(\frac{\hbar\omega_L}{k_B T} \right)^2 \sum_{n=1}^{\infty} n \exp\left(\frac{-n\hbar\omega}{k_B T} \right) g(\omega) d\omega. \quad (7)$$

Since the exponential factor in Eq. (7) will cut out contributions from all except small values of ω and T , we need to consider only the low frequency end of the phonon spectrum. Furthermore, for small values of ω , the phonon spectrum of a three-dimensional crystal has the expansion

$$g(\omega) = a_2 \omega^2 + a_4 \omega^4 + \dots \quad (8)$$

When this expansion is substituted into Eq. (7), and the upper limit on the integral is removed to infinity, we find that

$$C_v(T) \approx 3rNk_B \left[\frac{4\pi^4}{15} \left(\frac{k_B T}{\hbar} \right)^3 a_2 + \frac{16\pi^6}{21} \left(\frac{k_B T}{\hbar} \right)^5 a_4 + \dots \right]. \quad (9)$$

On the other hand, the Debye approximation for the phonon spectrum of a solid can be expressed as

$$g(\omega) = \frac{3\omega^2}{\omega_D^3}, \quad 0 \leq \omega \leq \omega_D, \quad (10)$$

$$g(\omega) = 0, \quad \omega > \omega_D.$$

It must be emphasized, however, that ω_D is an artificial limiting frequency which leads to correct normalization of $g(\omega)$ and bears no simple relation to the true maximum frequency of the crystal. Since the specific heat at low frequencies is mainly a function of the small ω behavior of $g(\omega)$ and the behavior of $g(\omega)$ in the Debye approximation and for exact discrete lattice models is the same for small ω , the Debye approximation can be accurately used for the analysis of the specific heat at low temperature and the estimation of the low frequency end of the phonon spectrum. Upon using the Debye characteristic temperature $\theta_D = \frac{\hbar\omega_D}{k_B}$, we find from Eqs. (10) and (6) that

$$C_V = 3rNk_B \left(\frac{T}{\theta_D}\right)^3 \int_0^{\frac{\theta_D}{T}} \frac{x^4 e^x dx}{(e^x - 1)^2}, \quad (11)$$

where $x = \frac{\hbar\omega}{k_B T}$ is a dimensionless parameter. In the limit where the upper limit on the integral in Eq. (11) can be removed to infinity, the expression of the specific heat reduces to

$$C_V = 3rNk_B \frac{4\pi^2}{5} \left(\frac{T}{\theta_D(0)}\right)^3, \quad (12)$$

which is the contribution of the lattice harmonic dynamics to the low temperature specific heat in Eq. (4). Moreover, we see from Eq. (11) that the specific heat of any solid in the Debye approximation is characterized by only one parameter $\frac{\theta_D}{T}$. Hence, in order to obtain accurate description of the solid specific heat, it is necessary to use a different value of θ_D at each temperature.^{18–20} The determination of the temperature dependence of θ_D can be done by equating the measured values of the specific heat to the Debye expression for the specific heat, Eq. (11), and consider the resulting equation as an equation for θ_D . The temperature-dependent θ_D of the surface-structured samples and that of the bare Si substrate are plotted together in Fig. 4 by using symbols. Now, comparing Eqs. (9) and (12), we see that

$$\frac{1}{\theta_D^3(0)} = \frac{k_B^3}{3\hbar^3} a_2, \quad (13)$$

where $\theta_D(0)$ is the Debye temperature at extremely low temperatures. On the other hand, Eq. (12) gives the rigorous low temperature specific heat of a crystal. However, in view of Eq. (9) if this is the case, θ_D must be a function of temperature whose value at any temperature is determined by equating Eqs. (12) and (6). When this is done, it is found that at low temperatures

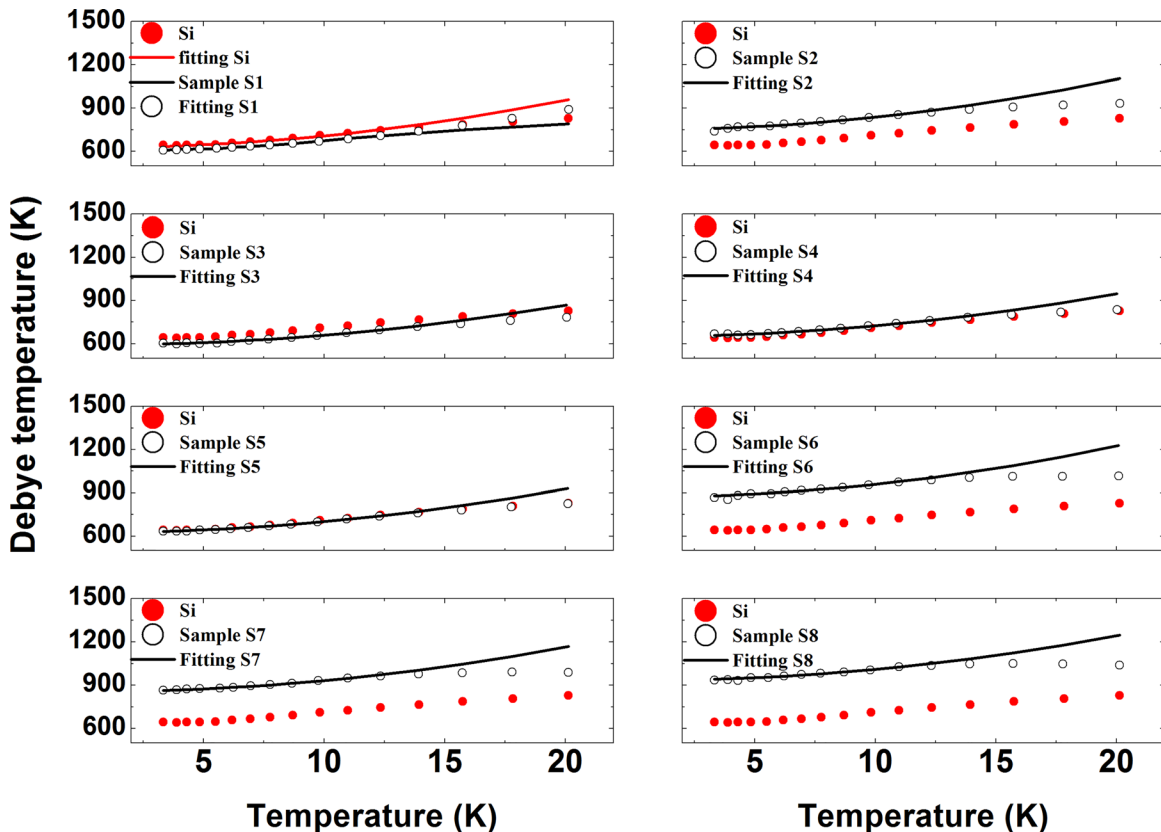


FIG. 4. Temperature-dependent Debye temperatures of the measured samples. Symbols: Values obtained by using the heat capacity measurements in Eq. (11). Solid lines: Best fits of the temperature-dependent Debye temperature curves with Eqs. (13) and (14).

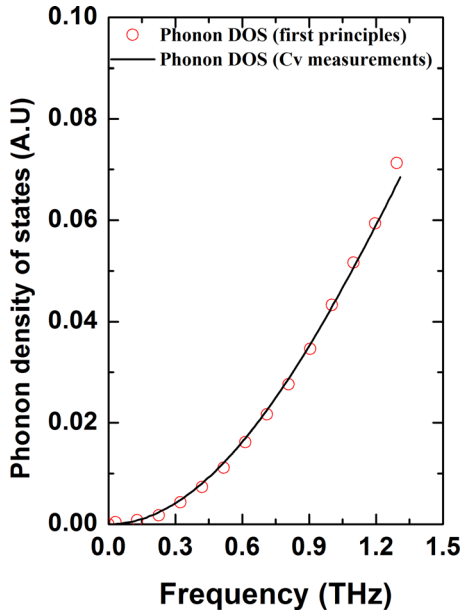


FIG. 5. Low frequency end of the phonon spectrum of Si. Symbols: Values obtained from the analysis of heat capacity measurements at low temperatures. Solid lines: Values obtained from first principles calculations.

$$\theta_D(T) = \theta_D(0) \left[1 - \frac{20\pi^2 a_4}{21 a_2} \left(\frac{k_B T}{\hbar} \right)^2 + \dots \right]. \quad (14)$$

The parameter $\theta_D(0)$ can be obtained by extrapolating the curves of $\theta_D(T)$ down to $T = 0$, and the coefficients of the low frequency end of the phonon spectrum (a_2 and a_4) can

be obtained by fitting the $\theta_D(T)$ curve with Eqs. (13) and (14). The best fits of $\theta_D(T)$ using Eqs. (13) and (14) are shown in Fig. 4 by solid lines, and the obtained values of $\theta_D(0)$, a_2 , and a_4 are reported in Table I. According to Eq. (8), the coefficients a_2 and a_4 can be used to plot the low frequency end of the phonon spectra of the measured samples.

In order to test the accuracy of the approach outlined above in determining the low frequency end of the phonon spectrum from a specific heat measurement, we have used it to determine the low frequency end of the phonon spectrum of the bare Si substrate and compared the results to first principle calculations of the phonon density of states of Si.^{21,22} The obtained curves are plotted together in Fig. 5 (after proper normalization). The good agreement between the derived and calculated phonon spectra at low frequencies clearly demonstrates the adequacy of the used experimental approach in determining the low frequency end of the phonon spectrum. The low frequency phonon spectra of the surface-structured samples as derived by using the approach described above are presented and compared to the bare Si substrate phonon spectrum in Fig. 6. It can be noticed that truncated cone-like structures of small height and broad apex (S4 and S5) do not alter the phonon spectrum at low frequencies. However, periodically arranged cone-like structures presenting sharp apexes (S1 and S3) enhance the phonon frequency, and periodically arranged pillar-like structures (S2) and tall truncated cone-like structures (S6–S8) weaken the phonon spectrum at low frequencies. The enhancement of the phonon spectrum at low frequencies is generally due to flatness in the low frequency acoustic phonon branches. This

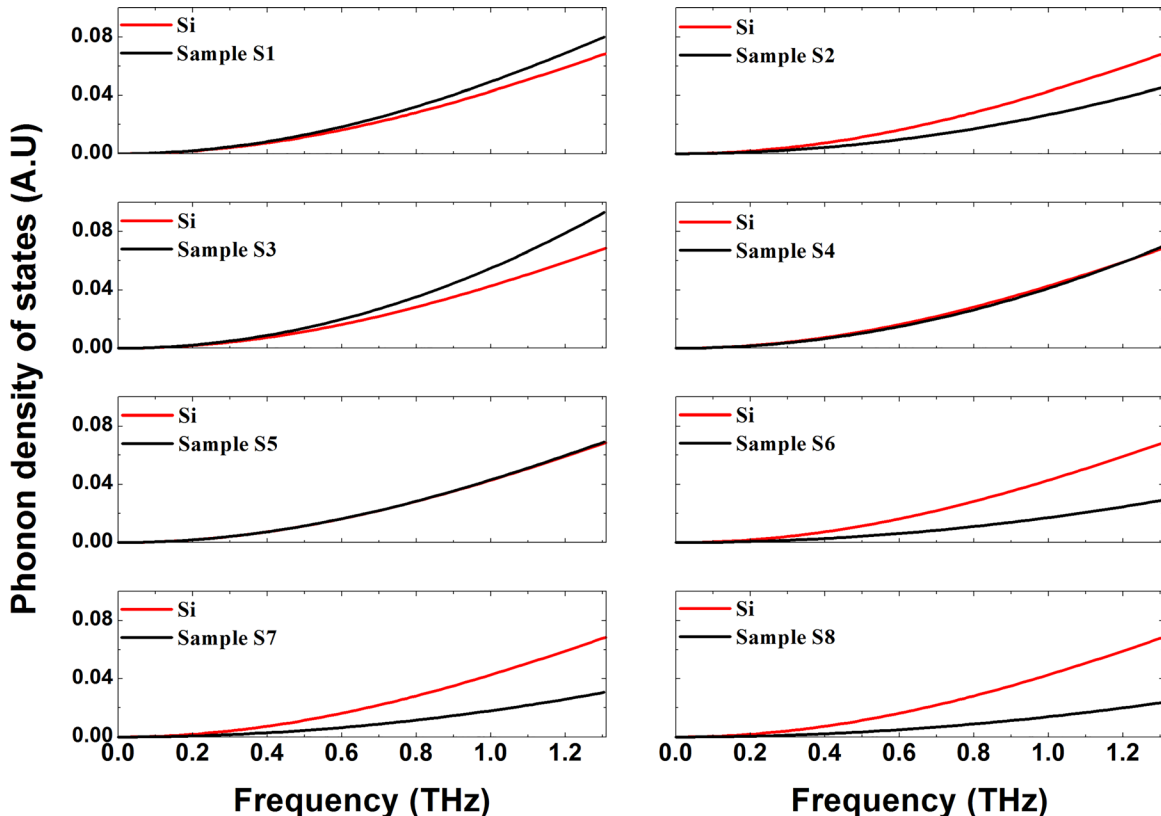


FIG. 6. Low frequency ends of the phonon spectra of the samples investigated.

is due to hybridization mechanisms between local resonances in the nanostructures made on the surface and the underlying low frequency bulk phonon modes.²³ The reduction in the phonon spectrum at low frequencies, on the other hand, is generally due to an enhancement of phonon modes frequencies. This may be attributed to a hybridization mechanism between non-localized acoustic phonon modes of degenerate dispersion relations in the nanostructures made on the surface and the underlying low frequency bulk phonon modes. Thus, cone-like structures of sharp apexes flatten the acoustic phonon branches and reduce the acoustic phonon group velocities due to a hybridization mechanism between local resonances (standing waves) and bulk phonon modes, whereas pillar-like structures and truncated cone-like structures of height exceeding 1 μm appear to have the effect of increasing the slopes of the acoustic phonon branches, and consequently increasing the acoustic phonon group velocities due to a hybridization mechanism between non-localized phonon modes (propagating waves) of degenerate dispersion relations in the nanostructures and low frequency bulk phonon modes. In the [Appendix](#), we make use of the Houston's method to show how the obtained coefficients of the low frequency end of the phonon spectrum are related to the phonon group velocities.²⁴

B. High frequency phonon spectrum from specific heat measurements

Now, let us see what conclusions about the high frequency phonon spectrum can be drawn from the analysis of the specific heat measurements at high temperatures. The Debye formula for heat capacity is developed based on a Debye-like density of states. Hence, it describes accurately the spectrum of only long wavelength phonons, which are excited at low temperatures. Therefore, the use of the Debye formula for heat capacity is appropriate to obtain information on the low frequency end of the phonon spectrum, but not on the spectrum of short wavelength phonons excited at high temperatures. The moment trace method, on the other hand, has been widely used for the approximate calculation of the phonon spectrum at high frequencies.^{25,26} The essence of this method is the expansion of $g(\omega)$ in a series of Legendre polynomials in which the coefficients of successive terms are linear combinations of the even spectrum moments, which are defined as

$$\begin{aligned}\mu_{2n} &= \frac{1}{3rN} \sum_{\mathbf{k}_j} \omega_j^{2n}(\mathbf{k}) = \frac{1}{3rN} \sum_{\mathbf{k}} \text{Tr} \mathbf{D}^n(\mathbf{k}) \\ &= \omega_L^{2n+1} \int_0^1 x^{2n} g(\omega_L x) dx,\end{aligned}\quad (15)$$

where $\mathbf{D}(\mathbf{k})$ is the dynamical matrix. It has been shown that the expansion in Legendre polynomials gives a fairly acceptable indication of the gaps in the phonon spectrum, a satisfactory description of the phonon spectrum at high frequency, and a poor description of the low frequency end of the phonon spectrum.²⁷ This can be understood if we realize that the low frequency end of the phonon spectrum is a slowly varying function of ω and would be poorly reproduced by a linear

combination of a few Legendre polynomials. Furthermore, the low frequency end of the phonon spectrum contributes very little to the moments, which is an additional reason this approximation might be expected to be a poor one at low frequencies. Therefore, the approximation presented below can be accurately employed for the calculation of the gaps in the spectrum and the phonon spectrum at high frequencies. We expand the phonon spectrum as

$$g(\omega) = \sum_{n=0}^{\infty} a_n P_n\left(\frac{\omega}{\omega_L}\right), \quad (16)$$

where the coefficients a_n are given by

$$a_n = (2n+1)^{-1} \int_{-1}^1 g(\omega_L x) P_n(x) dx. \quad (17)$$

Since $g(\omega)$ is an even function of ω , only the even coefficients a_{2n} are non-vanishing. The even moments of the phonon spectrum may be given in terms of the dimensionless moments u_{2n} as

$$\int_0^1 x^{2n} g(\omega_L x) dx = \frac{u_{2n}}{\omega_L}. \quad (18)$$

Since $P_{2n}(x)$ contains only even power of x , we find upon combining Eqs. (17) and (18) that the coefficient a_{2n} in Eq. (16) can be expressed as

$$\omega_L a_{2n} = \frac{2}{4n+1} P_{2n}(x)|_{x^2=u_{2n}}. \quad (19)$$

Thus, the approximate calculation of the phonon spectrum at high frequency can be made possible when the dimensionless spectrum moments u_{2n} are determined.

Thirring made use of the moments of the phonon spectrum to find an expansion for the specific heat at high temperatures in inverse powers of the temperature.²⁸ He used the result

$$\frac{x}{e^x - 1} = 1 - \frac{x}{2} - \sum_{n=1}^{\infty} (-1)^n B_{2n} \frac{x^{2n}}{(2n)!}, \quad |x| < 2\pi, \quad (20)$$

where B_{2n} are the Bernoulli numbers, to expand the second term on the right hand in the expression of the total energy

$$E(T) = \sum_{j=1}^{3rN} \left\{ \frac{\hbar\omega_j(k)}{2} + \frac{\hbar\omega_j(k)}{\exp\left(\frac{\hbar\omega_j(k)}{k_B T}\right) - 1} \right\}. \quad (21)$$

Then, upon interchanging the order of summations, Thirring found that

$$\begin{aligned}C_v(T) &= \left(\frac{\partial E(T)}{\partial T} \right)_v \\ &= (3rNk_B) \left[1 - \sum_{n=1}^{\infty} (-1)^n B_{2n} \frac{(1-2n)}{(2n)!} \left(\frac{\Theta}{T} \right)^{2n} u_{2n} \right],\end{aligned}\quad (22)$$

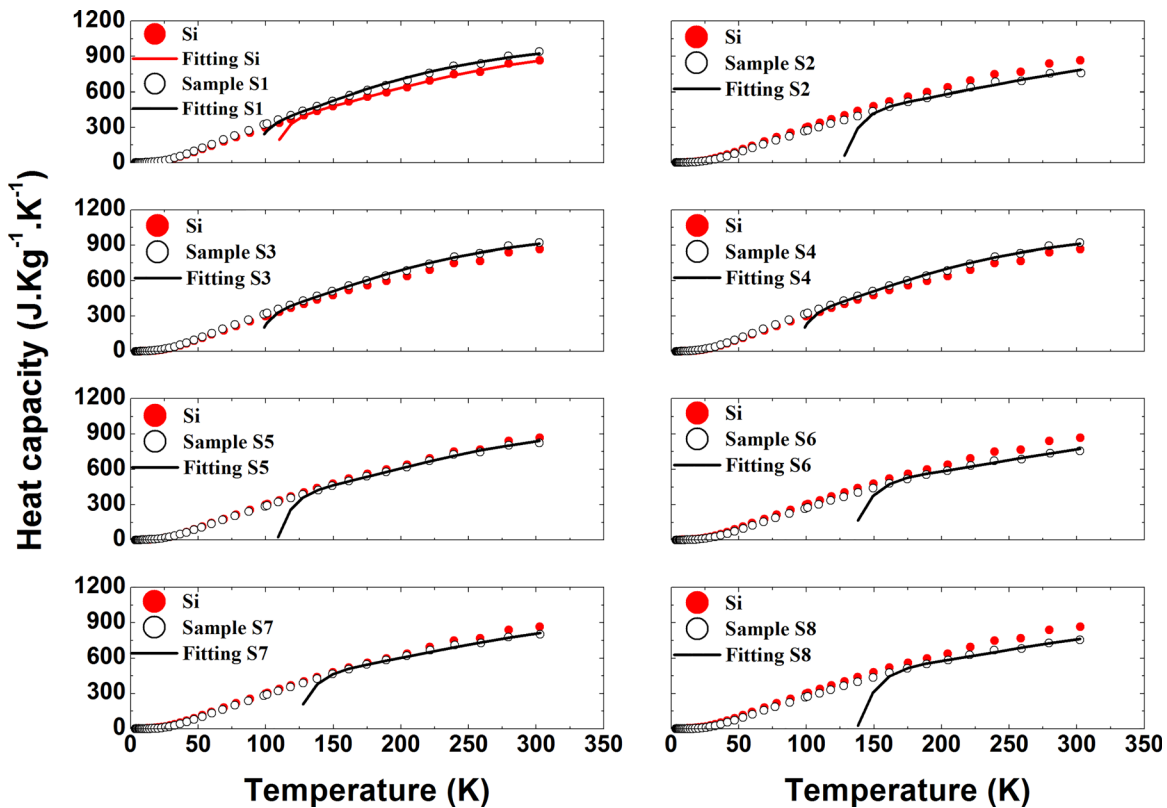


FIG. 7. Heat capacity. Symbols: measurements of the investigated samples. Solid lines: Best fit of the heat capacity measurements at high temperatures using Eq. (22).

where the parameter $\Theta = \frac{\hbar\omega_L}{k_B}$ bears no simple relation to the Debye temperature. By using Eq. (22), Thirring clearly demonstrated that one can find a high temperature expansion for the specific heat which converges, theoretically, for $T \gg \frac{\Theta}{2h}$. This limitation is imposed by the finite radius of convergence of the series in Eq. (20).

The moments of the phonon spectrum can hence be obtained by fitting Eq. (22) to the measured specific heat curves at high temperatures. Then, from the knowledge of the spectrum moments, the high frequency phonon spectrum can be approximated by using Eqs. (16) and (19). The best fits of Eq. (22) to the measured specific heat curves are shown in Fig. 7 in solid lines. This curve fitting technique allowed deducing only three spectrum moments for each measured samples. The obtained moments are presented in Table I. The fact that each investigated sample is characterized by a different spectrum moments set suggests that, besides the low frequency end of the phonon spectrum, the phonon spectrum at high frequencies can also be modified by surface structuration. Unfortunately, three moments were not sufficient to precisely describe the entire features of the phonon spectrum at high frequencies. In fact, it has been shown that at least fourteen spectrum moments are required to synthesize the main gaps in the high frequency phonon spectrum.²⁷ However, we believe that fitting Eq. (22) to specific heat curves in the full temperature range (up to a temperature close to the material melting point) might provide enough spectrum moments for accurate experimental description of the phonon spectrum at high frequencies. Such studies are under consideration.

IV. CONCLUSION

In summary, we have measured the heat capacities of bare and surface-structured Si substrates originated from the same Si wafer over 3–300 K temperature range. The results showed that the heat capacity curves of the surface-structured substrates significantly differ from that of the bare Si substrate in many aspects. We attributed this difference to an important modification in the phonon spectrum due to a phonon hybridization mechanism. In order to determine the phonon spectra of the measured samples at low frequencies, we took advantage of the fact that at low temperatures the expression for the heat capacity contains an exponential factor that cuts out contributions from all except small values of frequency and temperature, and expanded the low frequency end of the phonon spectrum in terms of polynomials of even coefficients. The obtained results showed that surface structuration may strongly modify the bulk phonon spectrum and group velocity of long wavelength phonons, which determine the elastic properties and are the principal heat carriers in semiconductor materials. We have also modeled the measured heat capacity at high temperatures by employing the Thirring's expansion technique, which consists in a formal high temperature expansion for the heat capacity in terms of the moments of the phonon spectrum. We have found that the surface structuration may also affect the phonon spectrum moments and, consequently, alter the phonon spectrum at high frequencies. Thus, the results presented in this paper clearly demonstrate the possibility of modifying mechanical, thermal, and infrared optical properties of bulk materials by

surface structuration and may open the door for the development of higher-performance technological metamaterials, either completely new or through surface structuration of existing ones.

ACKNOWLEDGMENTS

A. Iskandar, M. Kazan, and M. Tabbal would like to acknowledge the financial support by the National Council for Scientific Research (CNRS-Lebanon) and Munib and Angela Masri Institute of Energy and Natural Resources. Research reported here was also supported by Champagne-Ardennes Region and the European Regional Development Fund through the SYNAPS (D201207251) project and the Nano'mat platform for the clean room facilities and use of specific equipment. M. Tabbal would like to thank the "Direction de l'Enseignement Supérieur de la Recherche et de l'Innovation, Région Champagne-Ardenne" for a fellowship at UTT.

APPENDIX: THE USE OF HOUSTON'S METHOD FOR DERIVING A RELATIONSHIP BETWEEN THE COEFFICIENTS OF THE LOW FREQUENCY END OF THE PHONON SPECTRUM AND THE PHONON GROUP VELOCITIES

The method of Houston for calculating the phonon spectra and, by extension, thermodynamic properties of cubic crystals has attracted a lot of interest, because it gives best results at the lowest frequencies and therefore is valuable for deriving an accurate relationship between the coefficients of the low frequency end of the phonon spectrum and the phonon group velocities in cubic crystals. The phonon spectrum of the j th phonon branch can be given by

$$g_j(\omega) = \left(\frac{2\omega}{3r(2\pi)^3} \right) v^{-1} \int \delta(\omega^2 - \omega_j(\mathbf{k})) d^3k, \quad (\text{A1})$$

where v is the volume of the first Brillouin zone, and the integral is carried out through the first Brillouin zone. If we change to spherical polar coordinates (k, θ, φ) and use the relation

$$\delta(f(x)) = \sum_i \frac{\delta(x - x_i)}{|f'(x_i)|}, \quad (\text{A2})$$

where $\{x_i\}$ are simple zeros of $f(x)$, Eq. (A1) is transformed into

$$g_j(\omega) = \frac{1}{3r(2\pi)^3 v} \int_0^\pi \sin \theta d\theta \int_0^{2\pi} d\varphi k_j^2(\omega, \theta, \varphi) \frac{dk_j(\omega, \theta, \varphi)}{d\omega}, \quad (\text{A3})$$

where $k_j(\omega, \theta, \varphi)$ is the solution to $\omega = \omega_j(k, \theta, \varphi)$. This means that the quantity $\frac{1}{3r(2\pi)^3 v} k_j^2(\omega, \theta, \varphi) dk_j(\omega, \theta, \varphi)$ is the frequency distribution function per unit solid angle for the j th branch of the total spectrum. Let us denote this quantity by $g_j(\omega, \theta, \varphi)$.

The idea behind the Houston's method is as follows. The function $g_j(\omega, \theta, \varphi)$ has cubic symmetry in θ and φ , because the normal mode frequencies are invariant against any real orthogonal transformation of axes which takes the crystal to itself. This means $g_j(\omega, \theta, \varphi)$ can be expanded in terms of Kubic harmonics which have the symmetry of the lattice:²⁹

$$g_j(\omega, \theta, \varphi) = \sum_{m=0}^{\infty} a_m(\omega) K_m(\theta, \varphi), \quad (\text{A4})$$

where $K_0 = 1$ and the prime on the summation means that the term corresponding to $m = 1$ is to be omitted from the summation. The K_m satisfies the orthogonality condition

$$\int_0^\pi \sin \theta d\theta \int_0^{2\pi} d\varphi K_m(\theta, \varphi) K_n(\theta, \varphi) = 4\pi \gamma_m \delta_{mn}, \quad (\text{A5})$$

where γ_m is a normalization constant and δ_{mn} is the usual Kronecker symbol. The first few γ_m and Kubic harmonics as well as the method for generating these functions are reported in Ref. 30. Now, if we substitute Eq. (A4) into Eq. (A3) and make use of Eq. (A5), we obtain

$$g_j(\omega) = 4\pi a_0(\omega). \quad (\text{A6})$$

To obtain the coefficient $a_0(\omega)$, Houston considered that there exist directions in reciprocal space along which the cubic crystal dynamical matrix factors into equations of low degree in ω^2 which can be solved exactly for ω as a function of the wavevector \mathbf{k} . These directions are high symmetry directions such as (100), (110), and (111) directions. Along these directions, the equation $\omega = \omega_j(k, \theta, \varphi)$ can be expressed as $\omega = \omega_j(k_s, \theta_s, \varphi_s)$. Since these equations can be inverted exactly to obtain k for simple enough models, it follows that we can obtain $g_j(\omega, \theta_s, \varphi_s)$ exactly for these special directions. If we then retain as many terms in Eq. (A4) as the number of directions (θ_s, φ_s) , the $a_m(\omega)$ in Eq. (A4) is given as the solution of a set of simultaneous linear equations whose coefficients are the values of $g_j(\omega, \theta, \varphi)$ along the direction (θ_s, φ_s) . In particular, if $g_j(\omega, \theta, \varphi)$ is known along the (100), (110), and (111) directions, it follows from Eqs. (A4)–(A6) that:

$$g_j(\omega) = \frac{4\pi}{35} \left[10g_j^A(\omega) + 16g_j^B(\omega) + 9g_j^C(\omega) \right], \quad (\text{A7})$$

where the superscripts A , B , and C stand for (100), (110), and (111), respectively. Indeed, the Houston's method can be used for the approximate evaluation of any integral of the form

$$J = \int_0^\pi \sin \theta d\theta \int_0^{2\pi} d\varphi I(\theta, \varphi), \quad (\text{A8})$$

provided that $I(\theta, \varphi)$ has cubic symmetry.

Since we are dealing here with the low frequency end of the phonon spectrum, we need to consider only the acoustic branches of the phonon spectrum. From the general form of

a three-dimensional dynamical matrix, one can readily find that the leading term in the expansion of $\omega_j^2(\mathbf{k})$ is of $O(k^2)$. For small values of \mathbf{k} , we must then have

$$\omega_j^2(\mathbf{k}) = C_j^2(\theta, \varphi)k^2 + D_j^2(\theta, \varphi)k^4 + \dots, \quad (\text{A9})$$

where the coefficients C_j and D_j have the symmetry of the lattice. Inverting Eq. (A9), we find the frequency distribution function per unit solid angle for the j th branch of the spectrum

$$g_j(\omega, \theta, \varphi) = \frac{1}{3rv} \frac{1}{(2\pi)^3} \left[\frac{\omega^2}{C_j^3(\theta, \varphi)} - \frac{5D_j^2(\theta, \varphi)}{2C_j^7(\theta, \varphi)} \omega^4 + \dots \right]. \quad (\text{A10})$$

Thus, from Eqs. (8), (A10), and (A3), we find that

$$a_2 = \frac{1}{3rv} \frac{1}{(2\pi)^3} \sum_j \int_0^\pi \int_0^{2\pi} \frac{\sin \theta d\theta d\varphi}{C_j^3(\theta, \varphi)}, \quad (\text{A11})$$

and

$$a_4 = -\frac{5}{2} \frac{1}{3rv} \frac{1}{(2\pi)^3} \sum_j \int_0^\pi \int_0^{2\pi} \frac{D_j^2(\theta, \varphi) \sin \theta d\theta d\varphi}{C_j^7(\theta, \varphi)}. \quad (\text{A12})$$

One can readily notice from Eq. (A9) that the coefficients $C_j(\theta, \varphi)$ are just the phonon group velocities for a given direction (θ, φ) of propagation. Thus, by applying the Houston's method to the evaluation of the integral in Eq. (A11), we find that the coefficients of the low frequency end of the phonon spectrum can be expressed in terms of the phonon group velocities as

$$a_2 = \frac{1}{3rv} \frac{1}{(2\pi)^3} \frac{4\pi}{35} \sum_j \left[\frac{10}{C_{j(100)}^3} + \frac{16}{C_{j(110)}^3} + \frac{9}{C_{j(111)}^3} \right], \quad (\text{A13})$$

where subscripts (hkl) on C_j indicate crystallographic directions.

- ¹S. G. Kandlikar, *Heat Transfer Eng.* **26**(8), 5 (2005).
- ²T. Açıkalın, S. M. Wait, S. V. Garimella, and A. Raman, *Heat Transfer Eng.* **25**(1), 4 (2004).
- ³D. Li, Y. Wu, P. Kim, L. Shi, P. Yang, and A. Majumdar, *Appl. Phys. Lett.* **83**, 2934 (2003).
- ⁴G. Chen, M. S. Dresselhaus, G. Dresselhaus, J. P. Fleurial, and T. Caillat, *Int. Mater. Rev.* **48**, 45 (2003).
- ⁵A. I. Boukai, Y. Bunimovich, J. Tahir-Kheli, J.-K. Yu, W. A. Goddard III, and J. R. Heath, *Nature* **451**, 168 (2008).
- ⁶A. I. Hochbaum, R. Chen, R. D. Delgado, W. Liang, E. C. Garnett, M. Najarian, A. Majumdar, and P. Yang, *Nature* **451**, 163 (2008).
- ⁷Z. T. Tian, S. Lee, and G. Chen, *J. Heat Transfer* **135**, 061605 (2013).
- ⁸H. Weyl, *Math. Ann.* **71**, 441 (1912).
- ⁹B. L. Davis and M. I. Hussein, *Phys. Rev. Lett.* **112**, 055505 (2014).
- ¹⁰L. Yang, N. Yang, and B. W. Li, *Nano Lett.* **14**, 1734 (2014).
- ¹¹N. Zen, T. A. Puurtinen, T. J. Isotalo, S. Chaudhuri, and I. J. Maasilta, *Nat. Commun.* **5**, 3435 (2014).
- ¹²P. Wang, F. Casadei, S. C. Shan, J. C. Weaver, and K. Bertoldi, *Phys. Rev. Lett.* **113**, 014301 (2014).
- ¹³Z. Y. Wei, J. K. Yang, K. D. Bi, and Y. F. Chen, *J. Appl. Phys.* **118**, 155103 (2015).
- ¹⁴Y. B. Jin, N. Fernez, Y. Pennec, B. Bonello, R. P. Moiseyenko, S. Hemon, Y. D. Pan, and B. Djafari-Rouhani, *Phys. Rev. B* **93**, 054109 (2016).
- ¹⁵H. Nonarvar and M. I. Hussein, *Phys. Rev. B* **93**, 081412 (2016).
- ¹⁶G. R. Stewart, *Rev. Sci. Instrum.* **54**, 1 (1983).
- ¹⁷J. S. Hwang, K. J. Lin, and C. Tien, *Rev. Sci. Instrum.* **68**, 94 (1997).
- ¹⁸M. Kazan and S. Volz, *J. Appl. Phys.* **115**, 073509 (2014).
- ¹⁹Z. Alameh and M. Kazan, *J. Appl. Phys.* **112**, 123506 (2012).
- ²⁰A. Iskandar, A. Abou-Khalil, M. Kazan, W. Kassem, and S. Volz, *J. Appl. Phys.* **117**, 125102 (2015).
- ²¹M. Kazan, *Appl. Phys. Lett.* **95**, 141904 (2009).
- ²²M. Kazan, *J. Heat Transfer* **133**, 112401 (2011).
- ²³S. Xiong, K. Sääskilähti, Y. A. Kosevich, H. Han, D. Donadio, and S. Volz, *Phys. Rev. Lett.* **117**, 025503 (2016).
- ²⁴W. V. Houston, *Rev. Mod. Phys.* **20**, 161 (1948).
- ²⁵E. W. Montroll, *J. Chem. Phys.* **10**, 218 (1942).
- ²⁶E. W. Montroll, *J. Chem. Phys.* **11**, 481 (1943).
- ²⁷E. W. Montroll and D. C. Peaslee, *J. Chem. Phys.* **12**, 98 (1944).
- ²⁸H. Thirring, *Phys. Z.* **14**, 867 (1913); **15**, 127, 180 (1914).
- ²⁹H. Bethe and F. C. von der Lorge, *Phys. Rev.* **71**, 612 (1947).
- ³⁰D. D. Betts, A. B. Bhatia, and M. Wyman, *Phys. Rev.* **104**, 37 (1956).